femington

Int. J. Clin. Res. Med. Sci. (2026) 1(4):1–15
Article ID: IJCRMS-2026-810

Tailoring Drug Release Kinetics in 3D-Printed PLA-PCL Blends: Influence of Copolymer Composition on Microstructure and Dissolution Behavior

Fenilkumar Patel
fenilkumarpatel02@gmail.com
Independent Researcher

Abstract

The development of personalized drug delivery systems requires precise control over the microstructural features that govern release kinetics. This paper investigates the structure-property relationships in 3D-printed binary blends of polylactic acid (PLA) and polycaprolactone (PCL) fabricated via fused deposition modeling (FDM) for tunable drug release applications. Filaments with varying PLA: PCL ratios (100:0, 75:25, 50:50, 25:75, and 0:100) were prepared by hot-melt extrusion, incorporating 10 wt% ibuprofen as a model pharmaceutical ingredient. The thermal, rheological, and mechanical properties of the filament feedstocks were characterized to establish printability windows for each composition. Printed specimens were analyzed for morphological features using scanning electron microscopy (SEM) and X-ray diffraction (XRD), revealing distinct phase separation patterns correlated with blend ratio. In vitro dissolution studies demonstrated that drug release profiles could be systematically modulated from burst release (pure PLA) to sustained release over 72 hours (pure PCL), with intermediate blends exhibiting biphasic or modulated release behavior associated with discrete dispersed domains in the 75:25 and 25:75 formulations and a co-continuous phase structure in the 50:50 formulation. Differential scanning calorimetry (DSC) characterized the thermal transitions and crystallinity of the polymer phases; water uptake and erosion were not directly measured in this study. The results establish experimental relationships among blend composition, material characteristics, processing conditions, and ibuprofen release behavior within the investigated formulations.

Keywords

• 3D Printing • Fused Deposition Modeling (FDM) • PLA-PCL Blends • Drug Release Kinetics • Hot-Melt Extrusion (HME) • Personalized Medicine

1. Introduction

Personalized healthcare accounts for differences in therapeutic response arising from genetic, physiological, and lifestyle variation among patients [1]. This principle also affects pharmaceutical formulation: drug delivery systems may need to accommodate individual dosing and release requirements [2]. Fused deposition modeling (FDM), a form of three-dimensional printing, makes it possible to manufacture dosage forms with deliberately selected geometries and release characteristics [3].

PLA and PCL are biodegradable polyesters frequently investigated for biomedical use. PLA can be obtained from renewable feedstocks and generally provides relatively high strength, although it degrades more rapidly than PCL. PCL is more flexible and degrades slowly, properties that can support prolonged

© 2026 Femington Academic Publishing. All rights reserved.

drug release. Combining the polymers therefore offers a way to adjust mechanical and degradation behavior across a range between those of the individual materials.

Adding an active pharmaceutical ingredient (API) to a printable polymer formulation creates several formulation constraints. Temperatures used during filament extrusion and printing must remain compatible with the drug's stability. Release is also affected by how the API is distributed, whether it is crystalline or amorphous, and how it interacts with the surrounding polymer. These factors link formulation structure to drug-release performance and must be considered when designing individualized dosage forms.

This study evaluates PLA-PCL blends of different compositions as matrices for controlled ibuprofen delivery. Ibuprofen was selected as the model drug because its thermal stability and dissolution characteristics are well documented. The work seeks to identify suitable processing conditions for drug-loaded filaments, examine the microstructures associated with the measured release profiles, and quantify relationships among blend ratio, processing conditions, and dissolution behavior. Together, these analyses describe the experimentally observed links between composition, structure, and release.

2. Related Work

The background relevant to PLA–PCL printed dosage forms spans polymer-blend compatibility and morphology, pharmaceutical FDM, hot-melt extrusion (HME), and mechanisms of drug dissolution and release [4]. The studies discussed below provide the context for the present investigation. Research on printed pharmaceutical forms has considered the effects of formulation composition, drug physical state, and release-modifying excipients. Work involving ibuprofen-containing printlets is particularly relevant at the formulation level, whereas broader reviews trace developments in pharmaceutical additive manufacturing. Here, the emphasis is on the association between PLA:PCL ratio, blend morphology, and experimentally measured release behavior.

2.1 Materials Science and Polymer Blending

Knowledge of blend morphology and phase behavior is central to the development of polymer-based release systems. Mohamed et al. examined FDM process variables relevant to printability. Rajan et al. assessed how processing conditions and material properties jointly affect the characteristics of printed parts. In related work, Boschetto and Bottini modeled dimensional accuracy and identified thermal gradients and shrinkage as important contributors. These findings provide context for selecting processing windows for the PLA-PCL formulations examined here.

Prior investigations have characterized the phase behavior of PLA-PCL blends [5]. Fortelny et al. described their limited thermodynamic compatibility and showed that two-phase morphologies can nevertheless be controlled to obtain useful material properties. Urquijo et al. linked processing route to changes in blend morphology and mechanical response, indicating that melt-processing conditions affect the resulting phase structure. Ostafinska et al. further showed that the relative viscosities of the two polymers influence the development of dispersed or co-continuous phases [6]. The composition-dependent changes reported by Solechan et al. provide additional comparisons for the present work [7].

2.2 Drug Release Kinetics and Modeling

Mathematical models are commonly used to characterize drug-release profiles and identify the transport processes that may govern release from polymer matrices. The zero-order, first-order, Higuchi, and Korsmeyer–Peppas models provide different descriptions of release behavior. The interpretation of their

fitted parameters, particularly the release exponent in the Korsmeyer–Peppas model, depends on the geometry of the dosage form and the assumptions underlying each model. Consequently, model selection should consider both goodness of fit and the physical applicability of the model to the system under investigation.

During hot-melt extrusion, processing temperature, residence time, and shear conditions can influence drug-polymer miscibility, drug distribution, and the physical state of the active pharmaceutical ingredient. These factors are particularly important for thermally sensitive drugs, for which excessive processing temperatures may cause degradation. The selection of extrusion conditions should therefore account for the thermal properties of both the polymer blend and the incorporated drug.

2.3 FDM-Based Pharmaceutical Manufacturing

FDM is used in pharmaceutical additive manufacturing because geometry, infill, and drug loading can be adjusted during production [8]. Mohamed et al. examined how FDM settings affect part quality and dimensional accuracy. Rajan et al. related process variables to material behavior and printed-part properties, identifying nozzle temperature, layer height, and print speed as factors associated with mechanical integrity and release. Boschetto and Bottini modeled dimensional accuracy and highlighted the need to manage thermal gradients and shrinkage. This literature informs the processing-window assessment and printing conditions applied to the drug-loaded PLA–PCL filaments in this study.

2.4 Hot-Melt Extrusion of Drug-Loaded Polymers

HME provides the drug-loaded filaments required for subsequent FDM. Patil et al. reviewed its pharmaceutical use, including the effects of processing temperature and screw speed on drug stability and distribution. Censi et al. discussed relevant formulation and process variables, such as polymer-drug miscibility, thermal degradation, and amorphization during processing [9]. Accordingly, extrusion conditions need to be selected for the particular drug-polymer combination so that the API remains stable and is distributed throughout the filament. These considerations guided preparation of the ibuprofen-containing PLA–PCL feedstocks.

2.5 Ibuprofen–Polymer Interactions

Ibuprofen is a weak acid, and its carboxylic acid functionality may form hydrogen bonds with the carbonyl groups present in aliphatic polyesters, including PLA and PCL [10]. Interactions of this type can affect API dispersion, recrystallization, and transport through the polymer phase. Patil et al. and Censi et al. identify drug solid state and polymer miscibility as factors relevant to release performance. The predominantly amorphous ibuprofen detected here agrees with the general observations in that literature. A possible interaction with polyester carbonyl groups is considered in Section 5.1; however, this study did not use FTIR, NMR, or another spectroscopic method to verify it directly.

2.6 Biodegradable Polymer Characterization and Drug Dissolution Mechanisms

Analysis of biodegradable polyesters and release from polymer matrices provides the basis for interpreting the dissolution data [11]. Paarakh et al. described the established zero-order, first-order, Higuchi, and Korsmeyer-Peppas models. Askarizadeh et al. considered how release exponents can be interpreted and which factors guide model selection. Work by Fortelny et al. and Ostafinska et al. addresses PLA/PCL phase structure, compatibility, toughness, and the influence of component viscosity on dispersed

versus co-continuous morphologies. Urquijo et al. and Solechan et al. further relate melt-processing conditions and composition to blend morphology. This body of work supports the interpretation of the composition–structure–release relationships discussed in Section 5.

The study brings these research areas together to examine how PLA-PCL composition and the resulting material structure are associated with drug release from FDM-printed specimens.

3. Materials and Methods

3.1 Materials

The materials were PLA 4043D (NatureWorks, USA; approximate molecular weight 120 kDa) and PCL CAPA 6500 (Perstorp, Sweden; molecular weight 50 kDa). Ibuprofen supplied by Sigma-Aldrich (USA) was used as the model drug. Before processing, each material was vacuum-dried at 40°C for 24 hours to remove adsorbed moisture.

3.2 Filament Preparation

Five PLA:PCL mass ratios were prepared: 100:0, 75:25, 50:50, 25:75, and 0:100. The pellets were weighed, mixed by hand, and combined with ibuprofen at 10 wt% of the total formulation. Each mixture was processed in a Filabot EX6 twin-screw hot-melt extruder (USA) at 60 rpm [12]. The extrusion temperature was selected separately for each formulation, spanning 160°C for neat PLA to 90°C for neat PCL [13]. A spooler collected the resulting filaments, whose diameter was 1.75 ± 0.1 mm. As detailed in Sections 3.2 and 3.3, both extrusion and printing temperatures were changed with composition to obtain printable material. Composition and processing temperature are therefore confounded in the experimental design. The measured differences cannot be assigned to composition alone; the findings describe the formulations under their selected processing conditions. A follow-up study should vary temperature independently at fixed blend ratios to separate these effects.

3.3 3D Printing

Specimens were cylindrical, with a diameter of 10 mm and a height of 4 mm. The designs were prepared in computer-aided design software and converted to print files using Simplify3D. Printing used a FlashForge Creator Pro FDM system fitted with a 0.4 mm nozzle [14]. The layer height, print speed, and infill were 0.2 mm, 30 mm/s, and 100%, respectively. Depending on formulation, the nozzle was operated between 210°C for pure PLA and 120°C for pure PCL. The build plate remained at 40°C.

3.4 Thermal Analysis

Differential scanning calorimetry (DSC) was performed on a TA Instruments Q2000 calorimeter. Samples (5-10 mg) were heated from -80°C to 200°C at 10°C/min under nitrogen atmosphere. Glass transition temperatures (Tg), melting temperatures (Tm), and enthalpies of fusion were determined from the thermograms. Crystallinity was calculated using the theoretical heat of fusion for 100% crystalline PLA (93 J/g) and PCL (139 J/g). The degree of crystallinity for each polymer component in the blends was calculated using the following approach. The melting endotherms of PLA and PCL were sufficiently separated in the thermograms (PLA: ~170°C; PCL: ~60°C), allowing integration of individual melting peaks without significant overlap. The crystallinity of PLA (X_{PLA}) and PCL (X_{PCL}) in the blends was

calculated as:

$$X_{\mathrm{PLA}} = \frac{\Delta H_{\mathrm{m,PLA}}}{w_{\mathrm{PLA}} \cdot \Delta H^{0}_{\mathrm{m,PLA}}} \times 100\% \tag{1}$$

$$X_{\mathrm{PCL}} = \frac{\Delta H_{\mathrm{m,PCL}}}{w_{\mathrm{PCL}} \cdot \Delta H^{0}_{\mathrm{m,PCL}}} \times 100\% \tag{2}$$

where $\Delta H_{\mathrm{m,PLA}}$ and $\Delta H_{\mathrm{m,PCL}}$ are the measured melting enthalpies of PLA and PCL in the blend, w_{PLA} and w_{PCL} are the weight fractions of PLA and PCL in the blend, and $\Delta H^{0}_{\mathrm{m,PLA}} = 93$ J/g and $\Delta H^{0}_{\mathrm{m,PCL}} = 139$ J/g are the theoretical heats of fusion for 100% crystalline PLA and PCL, respectively. The melting enthalpies were determined by integrating the area under the respective endothermic peaks using the instrument software. In cases where minor overlap occurred at the baseline, a linear baseline correction was applied between the onset and offset temperatures of each melting transition.

3.5 Rheological Characterization

Melt rheology was assessed on an Anton Paar MCR 302 using 25 mm parallel plates. At temperatures matching the respective printing conditions, frequency sweeps were recorded from 0.1 to 100 rad/s within the linear viscoelastic region.

3.6 Mechanical Testing

An Instron 5965 universal testing machine fitted with a 1 kN load cell was used to determine tensile properties. Type V dog-bone specimens conforming to ASTM D638 were printed and tested at a crosshead rate of 5 mm/min. Each composition was evaluated using five specimens.

3.7 Morphological Characterization

Cross-sections of printed specimens were examined using scanning electron microscopy (SEM) (Hitachi S-4800) after gold sputter coating. Phase separation was visualized using backscattered electron imaging. Image analysis software was used to quantify domain sizes and distribution. SEM images were acquired at magnifications of 500×, 1000×, and 2000× to visualize phase morphology at different length scales. For quantitative domain-size analysis, images at 2000× magnification were used. Image segmentation was performed using ImageJ software (National Institutes of Health, USA). A minimum of 100 domains per composition were analyzed from at least five independent images. Domain sizes were measured as the equivalent circular diameter, calculated from the measured area of each domain. It is important to clarify that the $n \geq 100$ domains analyzed per composition represent technical measurements from a single experimental batch and do not constitute independent experimental replicates. The five independent images were acquired from different regions of the same printed specimen. True experimental replication would require independent fabrication and processing runs, which was not performed in this study. The domain size values reported in Table 4 therefore describe the morphological characteristics of the specific specimens analyzed and may not capture batch-to-batch variability. Future work should include independent replicate batches to assess reproducibility. The number-average domain diameter (D_n) and volume-average domain diameter (D_v) were calculated as:

$$D_n = \frac{\sum n_i D_i}{\sum n_i} \tag{3}$$

$$D_v = \frac{\sum n_i D_i^4}{\sum n_i D_i^3} \tag{4}$$

where n_i is the number of domains with diameter D_i.

3.8 X-Ray Diffraction

A Bruker D8 Advance diffractometer was used to acquire X-ray diffraction patterns with Cu Kα radiation (λ = 1.5406 Å). Scans covered 2θ = 5-40° at 2°/min. The patterns were examined to determine whether ibuprofen in the polymer matrices was crystalline or amorphous.

3.9 In Vitro Dissolution Studies

The dissolution protocol used a USP II paddle system (Distek 2100B) containing 900 mL of phosphate buffer at pH 7.4. The temperature was held at 37 ± 0.5°C and the paddles rotated at 50 rpm [15]. Printed specimens were immersed (defined as the initial baseline time point t = 0 h with 0% cumulative release), and aliquots of 5 mL were collected at 0.5, 1, 2, 4, 8, 12, 24, 48, and 72 hours. The removed volume was replaced with an equal volume of fresh phosphate buffer maintained at 37°C to maintain constant dissolution medium volume. UV-Vis spectrophotometry at 264 nm was used to quantify ibuprofen. A calibration curve was prepared by dissolving ibuprofen in phosphate buffer (pH 7.4) at concentrations ranging from 5 to 100 µg/mL. The absorbance at 264 nm was linear over this range ($R^2 > 0.999$). The ibuprofen concentration in each sample was determined from the calibration curve. Cumulative drug release was calculated as the percentage of the total ibuprofen content in each specimen. The theoretical drug loading (10 wt%) was used to calculate the total ibuprofen content because the actual drug content was not independently measured for each specimen; this represents a limitation of the study. Sink conditions were maintained throughout the dissolution experiments, as the maximum ibuprofen concentration in the medium (approximately 100 µg/mL) remained well below the solubility limit of ibuprofen in phosphate buffer at pH 7.4. Three independent dissolution runs were completed for each formulation (n=3). Results are expressed as mean ± standard deviation. Release profiles were compared by one-way ANOVA with Tukey's post-hoc procedure; statistical significance was set at $p < 0.05$.

4. Results and Discussion

4.1 Filament Processing and Printability

FDM feedstock must maintain a consistent diameter and combine enough flexibility for feeding with sufficient stiffness to prevent buckling. Extrusion yielded filaments within acceptable dimensional tolerances across the tested formulations. The usable processing-temperature range became narrower as the PCL fraction increased, consistent with the lower melting temperature and thermal stability of PCL.

Neat PCL filaments were tacky and insufficiently stiff, which made feeding less reliable during printing. Incorporating at least 25% PLA improved filament handling, suggesting that PLA contributed reinforcement to the feedstock.

4.2 Thermal Properties

The DSC thermograms contained separate transitions attributable to the two polymers [16]. For PLA, the glass transition occurred near 60°C and the melting endotherm near 170°C. PCL showed a melting

transition at approximately 60°C; its glass transition was not distinguishable within the temperature range examined.

As the PCL fraction rose, the PLA glass-transition temperature shifted downward slightly, which may reflect limited miscibility near the phase boundary. PCL was more crystalline in the blends than in the neat material, a trend consistent with a possible nucleating effect from PLA. In contrast, adding PCL reduced PLA crystallinity, potentially because the rubbery phase restricts PLA chain mobility [17]. Table 1 reports the thermal measurements for each blend. Component crystallinities were obtained from Eqs. (1) and (2). One-way ANOVA with Tukey's post-hoc comparisons indicated composition-dependent differences for both polymers ($p < 0.05$ for every pairwise comparison).

Table 1: Thermal properties of PLA–PCL blends (mean ± standard deviation, $n = 3$ independent measurements)

PLA:PCL	T_g **PLA (°C)**	T_m **PLA (°C)**	T_m **PCL (°C)**	X_{PLA} **(%)**	X_{PCL} **(%)**
100:0	60.2 ± 0.5	170.1 ± 0.8	–	38.5 ± 1.2	–
75:25	59.8 ± 0.4	169.5 ± 0.7	59.2 ± 0.5	35.2 ± 1.1	42.8 ± 1.5
50:50	59.1 ± 0.5	168.8 ± 0.9	58.8 ± 0.6	31.8 ± 1.3	45.6 ± 1.8
25:75	58.5 ± 0.4	168.2 ± 0.8	58.5 ± 0.5	28.4 ± 1.0	48.2 ± 1.6
0:100	–	–	58.0 ± 0.6	–	52.5 ± 1.9

4.3 Rheological Behavior

All formulations showed shear-thinning, as indicated by the decrease in complex viscosity with increasing angular frequency. Neat PLA had the greatest viscosity and neat PCL the smallest; the blends fell between these limits according to their composition.

Rheology was reflected in the behavior of the deposited material. Neat PLA and the 75:25 blend retained their shape after extrusion, although their higher viscosity required greater extrusion pressure. By comparison, the 25:75 blend and neat PCL flowed more readily but showed some sagging after deposition. Table 2 lists the complex viscosity measured at 10 rad/s. One-way ANOVA followed by Tukey's test found significant differences among all compositions ($p < 0.05$).

Table 2: Complex viscosity of PLA–PCL blends at 10 rad/s (mean ± standard deviation, $n = 3$ independent measurements)

PLA:PCL	**Complex Viscosity (Pa·s)**
100:0	1250 ± 85
75:25	820 ± 62
50:50	540 ± 45
25:75	310 ± 28
0:100	185 ± 18

4.4 Mechanical Properties

The tensile response changed markedly across the blend series. Neat PLA was relatively stiff and fractured at low strain, whereas neat PCL combined a lower modulus with much greater elongation. The intermediate formulations exhibited mechanical responses between these two end members [18].

The mechanical properties are summarized in Table 3.

Table 3: Mechanical properties of PLA-PCL prints

PLA:PCL	Tensile Strength (MPa)	Young's Mod (MPa)	Elongation (%)
100:0	58.3 ± 3.2	2850 ± 120	4.2 ± 0.8
75:25	42.1 ± 2.8	1950 ± 95	15.8 ± 2.1
50:50	28.6 ± 2.1	1120 ± 80	42.3 ± 4.5
25:75	18.4 ± 1.6	540 ± 45	210 ± 18
0:100	12.5 ± 1.2	280 ± 30	580 ± 45

Mechanical behavior is relevant to the handling and physical integrity of printed dosage forms. A higher modulus can help a specimen resist deformation during storage and handling, whereas ductility may affect how the printed structure responds during dissolution-associated swelling or erosion.

4.5 Morphological Characterization

The SEM micrographs showed composition-dependent phase arrangements, in agreement with the morphology reported for related blends [19]. Each neat polymer appeared as a single homogeneous phase, whereas the mixed formulations separated into domains. In the 75:25 material, PCL formed dispersed domains within a continuous PLA phase; the number-average diameter was 1.2 ± 0.4 μm. At 50:50, the two phases were interpenetrating and co-continuous, with a domain size of 2.5 ± 0.8 μm. The 25:75 blend instead contained discrete PLA domains in a continuous PCL matrix, and its number-average diameter was 3.8 ± 1.2 μm. Across the blends, measured domains spanned 0.5-5 μm; the larger domains occurred at higher PCL fractions.

Table 4 reports the number-average diameter (D_n) and volume-average diameter (D_v) for each blend. Distribution breadth was expressed as a domain-size ratio, calculated from D_v/D_n.

The measured domain-size distributions varied across the investigated PLA–PCL compositions. These differences are presented descriptively because the measurements were obtained from multiple regions of a single fabricated batch per composition. The individual domain measurements do not constitute independent experimental replicates; therefore, inferential statistical comparisons between compositions were not performed. Independent fabrication batches would be required to establish the reproducibility and statistical significance of the observed morphological differences.

Table 4: Quantitative morphological analysis of PLA–PCL blends (mean ± standard deviation, $n \geq 100$ domains from ≥ 5 independent images per composition)

PLA:PCL	D_n (μm)	D_v (μm)	Domain-size ratio (D_v/D_n)	Morphology
100:0	–	–	–	Homogeneous
75:25	1.2 ± 0.4	1.8 ± 0.6	1.5	Discrete PCL domains
50:50	2.5 ± 0.8	3.9 ± 1.2	1.6	Co-continuous
25:75	3.8 ± 1.2	5.7 ± 1.8	1.5	Discrete PLA domains
0:100	–	–	–	Homogeneous

The morphology data in Table 4 came from one fabricated batch for each composition. Although at least 100 domains were measured per formulation, these are technical observations taken from several regions of the same specimen, not independent batch replicates. Thus, the comparisons characterize the specimens examined and cannot establish between-batch reproducibility. Replicated fabrication runs are needed to determine whether the measured morphology is consistent across batches.

Changes in phase continuity may help explain the differences in release profiles. In a co-continuous

material, both polymer phases may contribute to fluid access and matrix loss, producing more complex release behavior. The continuous PLA phase in the 75:25 blend is consistent with its early burst, whereas a continuous PCL phase in the 25:75 formulation is consistent with slower release. These are mechanistic interpretations rather than directly measured transport processes.

4.6 Drug Physical State

The diffraction patterns indicated that ibuprofen was predominantly amorphous in each printed formulation. Peaks normally associated with crystalline ibuprofen, at approximately 16.8°, 20.1°, and 22.3° 2θ, were not detected. This finding suggests substantial drug amorphization during extrusion and printing. It does not, however, establish that every ibuprofen molecule was amorphous: the approximate crystallinity detection limit of XRD is 5%. Consistent with the diffraction data, DSC thermograms showed no melting endotherm in the 75–78°C range typically associated with crystalline ibuprofen. Taken together, the two methods support the conclusion that the drug was present mainly in an amorphous form.

An amorphous drug phase can dissolve without first undergoing crystal-lattice disruption, which may favor dissolution. This physical state can be unstable, however, and recrystallization during storage could change subsequent release. Confinement within the polymer and possible molecular interactions may limit that process.

4.7 Dissolution Studies

The dissolution measurements varied with PLA:PCL ratio. At 24 hours, one-way ANOVA indicated a statistically significant overall effect of formulation composition on cumulative drug release ($p < 0.05$). The neat PLA specimens released 68 ± 4% of their ibuprofen by 4 hours and 94 ± 3% by 24 hours (Table 5). This rapid profile may be associated with fluid ingress into the amorphous PLA matrix and matrix erosion. Neither water uptake nor erosion was measured directly, however. These explanations are therefore hypotheses informed by the release data and previously reported PLA degradation behavior; dedicated measurements would be needed to test them.

Neat PCL released ibuprofen more gradually: 28 ± 2% had been released at 24 hours and 68 ± 4% at 72 hours (Table 5). Its hydrophobic character and resistance to hydrolytic degradation are consistent with this slower profile.

The mixed formulations produced release profiles between those of neat PLA and neat PCL, with the exact pattern depending on blend ratio. For the 75:25 formulation, 42 ± 3% was released during the first 4 hours; release then proceeded more slowly, reaching 82 ± 4% at 24 hours and 96 ± 2% at 72 hours. The 50:50 blend approached a linear profile over 48 hours, with approximately 62 ± 4% released by 24 hours and 78% by 48 hours. Nevertheless, the best statistical fit was obtained with the Korsmeyer–Peppas expression ($R^2 = 0.993$, $n = 0.45$). The profile should therefore not be interpreted as strictly zero-order; diffusion and polymer relaxation may both contribute. The 25:75 blend released 8 ± 1% by 4 hours and 38 ± 3% by 24 hours, retaining a sustained pattern similar to neat PCL but with a somewhat faster early release.

Selected cumulative-release measurements at 4, 24, and 72 hours appear in Table 5. Following the significant overall one-way ANOVA ($p < 0.05$), Tukey's post-hoc pairwise comparisons at 24 hours revealed statistically significant differences between all formulation pairs ($p < 0.05$), except for the comparison between the 25:75 and 0:100 formulations, which did not reach statistical significance ($p = 0.08$).

Figure 1 presents the cumulative ibuprofen-release curves for the five formulations.

Table 5: Cumulative ibuprofen release (%) at selected time points (mean ± standard deviation, $n = 3$ independent replicates)

PLA:PCL	4 h	24 h	72 h
100:0	68 ± 4	94 ± 3	99 ± 1
75:25	42 ± 3	82 ± 4	96 ± 2
50:50	22 ± 2	62 ± 4	88 ± 3
25:75	8 ± 1	38 ± 3	72 ± 4
0:100	4 ± 1	28 ± 2	68 ± 4

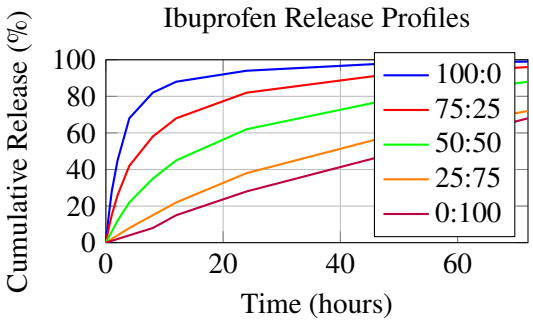


Figure 1: Cumulative ibuprofen release profiles from printed PLA-PCL blends. Error bars represent standard deviation from three independent dissolution runs.

4.8 Kinetic Modeling

Four kinetic expressions were evaluated against the dissolution data: zero-order ($M_t/M_\infty = k_0 t$), first-order ($M_t/M_\infty = 1 - e^{-k_1 t}$), Higuchi ($M_t/M_\infty = k_H t^{1/2}$), and Korsmeyer–Peppas ($M_t/M_\infty = k t^n$). In addition to the initial baseline observation at $t = 0$ h (0% cumulative release), samples were collected at 0.5, 1, 2, 4, 8, 12, 24, 48, and 72 hours (Section 3.9). Fits were restricted to observations within the 0–60% cumulative-release interval, including the $t = 0$ h initial condition. Based on the actual cumulative-release data, the included intervals were 0–2 h for 100:0 (4 observations: 0, 0.5, 1, and 2 h), 0–8 h for 75:25 (6 observations: 0, 0.5, 1, 2, 4, and 8 h), 0–12 h for 50:50 (7 observations: 0, 0.5, 1, 2, 4, 8, and 12 h), 0–48 h for 25:75 (9 observations: 0, 0.5, 1, 2, 4, 8, 12, 24, and 48 h), and 0–48 h for 0:100 (9 observations: 0, 0.5, 1, 2, 4, 8, 12, 24, and 48 h). The coefficient of determination (R^2) and Akaike Information Criterion were used for model assessment; AIC was calculated as $\mathrm{AIC} = N \ln(\mathrm{RSS}/N) + 2p$, where N denotes the number of observations, RSS the residual sum of squares, and p the number of fitted parameters. The preferred model was the one combining the lowest AIC with the highest R^2.

Model selection across the zero-order, first-order, Higuchi, and two-parameter Korsmeyer–Peppas expressions was evaluated directly via R^2 and AIC across the same observations for each formulation, accounting for differences in parameter count (p) through the AIC penalty term. Standard errors for k and n were also obtained from the covariance matrix of each nonlinear least-squares fit. Table 6 gives the R^2 and AIC results for the four models and five compositions.

Among the four expressions, Korsmeyer–Peppas gave the strongest fit for every blend. Its AIC values were the lowest (from −44.2 to −40.8), while its R^2 values were the highest (0.989-0.994) relative to the zero-order, first-order, and Higuchi alternatives. The fitted release exponent n also changed consistently with PLA:PCL ratio.

The fitted parameters are listed in Table 7.

Table 7 contains two different measures of uncertainty. The “mean ± SD” values summarize the mean

Table 6: Model comparison for ibuprofen release from PLA–PCL blends

PLA:PCL	Zero-order		First-order		Higuchi		Korsmeyer–Peppas	
	R^2	AIC	R^2	AIC	R^2	AIC	R^2	AIC
100:0	0.812	−18.4	0.876	−22.1	0.934	−28.7	0.991	−42.3
75:25	0.798	−17.2	0.861	−21.4	0.921	−27.5	0.989	−40.8
50:50	0.781	−16.5	0.849	−20.8	0.908	−26.2	0.993	−43.1
25:75	0.764	−15.8	0.832	−19.6	0.892	−24.9	0.992	−41.7
0:100	0.749	−15.1	0.818	−18.9	0.876	−23.4	0.994	−44.2

Table 7: Release kinetic parameters from the Korsmeyer–Peppas model. Values in the "mean ± SD" columns are the mean and standard deviation of the fitted parameters across $n = 3$ independent dissolution replicates. Values in the "SE" columns are the standard errors of the fitted parameters obtained from the covariance matrix of the nonlinear least-squares regression, reported separately as a distinct statistical quantity.

PLA:PCL Ratio	k (h^{-n})	SE(k)	n	SE(n)	R^2
100:0	0.32 ± 0.02	0.01	0.52 ± 0.01	0.005	0.991
75:25	0.24 ± 0.02	0.01	0.48 ± 0.01	0.005	0.989
50:50	0.15 ± 0.01	0.005	0.45 ± 0.01	0.004	0.993
25:75	0.08 ± 0.01	0.004	0.43 ± 0.01	0.004	0.992
0:100	0.04 ± 0.00	0.002	0.41 ± 0.01	0.003	0.994

and standard deviation of k and n across the three independent dissolution replicates, with the model fitted separately to each replicate. They therefore describe variation between runs. The "SE" columns instead give parameter standard errors calculated from the covariance matrix of the nonlinear least-squares fit and represent within-fit estimation precision. Reported R^2 values are averages across the three replicates. Differences in n among compositions were tested by one-way ANOVA and Tukey's post-hoc procedure, using $p < 0.05$ as the significance criterion. The exponent declined as PCL content increased; each adjacent-composition comparison was statistically significant ($p < 0.05$).

The fitted release exponent varied across the investigated compositions. The interpretation of the exponent requires consideration of the cylindrical geometry of the printed specimens and the assumptions of the Korsmeyer–Peppas model. Although the observed values may indicate differences in the relative contributions of diffusion and polymer relaxation, the fitted exponents alone do not establish the underlying release mechanism. In particular, polymer erosion was not directly measured in this study. Therefore, the exponent values are interpreted as empirical descriptors of the release profiles rather than definitive evidence of specific transport mechanisms. The composition-dependent changes in k and n quantify the observed association between blend ratio and release kinetics.

5. Discussion

5.1 Structure-Property Relationships

The measurements connect blend ratio with phase morphology and the resulting release profile. Because PLA and PCL are immiscible, the blends separate into phases whose arrangement depends on the proportion of each polymer [4]. In the present series, co-continuity was observed near the 50:50 composition, suggesting that phase continuity changes around this ratio. The discussion below distinguishes direct observations from explanations that remain hypotheses.

Observed results: Relative to neat PCL, PCL crystallinity was higher in the blends; PLA crystallinity declined as PCL was added (Table 1). Release was faster in PLA-rich formulations and slower in those containing more PCL.

Proposed mechanisms: Crystallinity may affect fluid penetration and drug transport through each polymer phase, but neither process was measured directly. The combination of increased PCL crystallinity and slower release in PCL-rich specimens may be consistent with stronger barrier behavior associated with the phase structure. Likewise, the lower PLA crystallinity observed after PCL addition may be related to the early release behavior of PLA-rich formulations. These explanations remain interpretations of the measured correlations. Measurements of water uptake, erosion, and drug diffusion would be needed to establish the proposed mechanisms.

This work did not directly quantify water absorption, polymer degradation, or erosion. The mechanisms discussed above are therefore possible interpretations of the release curves, informed by established knowledge of PLA and PCL. Experimental measurements of these processes are required before the proposed explanations can be confirmed.

Observed results: XRD and DSC analysis confirmed that ibuprofen existed predominantly in an amorphous state within all printed formulations (Section 4.5).

Proposed mechanisms: Because the drug was predominantly amorphous, dissolution of an intact crystal is unlikely to be the controlling step; transport through the polymer matrix may instead govern the measured profiles. Hydrogen bonding between the ibuprofen carboxylic acid group and polyester carbonyl groups is another possible contributor. No spectroscopic measurements were performed to verify this interaction. It is proposed from the chemical structures alone and requires direct evidence, for example from FTIR or NMR.

5.2 Processing-Structure Correlations

Observed results: Extrusion and printing settings changed with blend composition (Section 3.2), and the resulting specimens showed composition-dependent morphology (Table 4).

Proposed mechanisms: The higher temperatures used for PLA-rich formulations may have increased melt flow and promoted mixing, whereas the lower settings for PCL-rich blends may have retained more distinct phase domains [20]. Extrusion shear may also affect domain dimensions and dispersion, with stronger shear potentially producing smaller domains. These effects cannot be isolated here because processing temperature and composition changed together (Section 3.2).

Observed results: Printability varied alongside the rheological measurements (Table 2). The formulations with complex viscosity in the 200-800 Pa·s range at printing shear rates (approximately 100 s^{-1}) showed the most favorable printing behavior.

Proposed interpretation: This viscosity interval may serve as an initial screening criterion for other formulations. Its broader applicability remains uncertain until it is tested with additional polymer systems.

5.3 Implications for Personalized Dosing

The measured dependence of release on blend ratio may help guide the formulation of dosage forms intended to deliver drug over selected time scales, although the proposed predictive use has not been validated independently [21]. PLA-rich matrices may be worth investigating for faster delivery, while PCL-rich materials may be candidates for release extending over several days. The approximately linear profile of the co-continuous blend could also be relevant to formulations designed to maintain drug

levels. However, the kinetic analysis did not establish strictly zero-order release. These are prospective applications, not demonstrated clinical outcomes.

FDM could, in principle, allow dose, geometry, and release behavior to be adjusted during dosage-form manufacture. This possibility has not been tested in clinical studies. Tablet dimensions and blend composition might eventually be varied to account for patient-related dosing requirements, while spatially separated regions made from different blends could be explored for pulsatile or biphasic delivery. Such designs remain prospective concepts and require experimental and clinical evaluation; they were not outcomes established by the present work.

6. Conclusion

This investigation quantified associations among composition, material structure, and ibuprofen release in FDM-printed PLA-PCL blends. The principal findings are:

1. PLA and PCL form immiscible blends with phase-separated morphologies that evolve from discrete domains to co-continuous structures as composition approaches 50:50.

2. Thermal processing conditions, rheological behavior, and mechanical properties varied across the investigated formulations. These observations provide descriptive information about the printability of the tested PLA–PCL blends under their respective processing conditions.

3. Ibuprofen exists predominantly in an amorphous state within printed matrices, and drug-polymer interactions are proposed as possible influences on distribution and release, although direct spectroscopic confirmation of these interactions was not performed in this study.

4. Release profiles varied systematically from rapid release (hours) to sustained release (days) across the tested formulations under their respective processing conditions, with the co-continuous 50:50 morphology exhibiting an approximately linear release profile over extended periods [22]. Because extrusion and printing temperatures were varied alongside blend ratio, these observed differences reflect the combined influence of formulation composition and processing conditions rather than composition alone; the use of release modifiers in FDM-printed dosage forms provides additional formulation context for tuning release behavior [8].

5. The Korsmeyer-Peppas model parameters k and n correlate with blend ratio, describing the experimentally observed composition–release relationship and providing a quantitative basis that may inform the design of dosage forms with tailored release profiles.

The results may inform future efforts to design 3D-printed dosage forms with selected release profiles, but the proposed predictive criteria and applications still require independent validation [3]. Further studies should test the relationships across independently prepared batches and other drug-polymer combinations, and assess multi-compartment constructs for more complex release patterns. Computational models and machine-learning methods could also be investigated as tools for formulation screening and for adapting printing settings to specified release targets.

References

[1] Margaret A Hamburg and Francis S Collins. The path to personalized medicine. *New England Journal of Medicine*, 363(4):301–304, 2010.

[2] Shashi Mathur and Joseph Sutton. Personalized medicine could transform healthcare. *Biomedical Reports*, 7(1):3–5, 2017.

[3] Tobias Auel, Aaron Felix Christofer Mentrup, Lee Roy Oldfield, and Anne Seidlitz. 3d printing of pharmaceutical dosage forms: Recent advances and applications. *Advanced Drug Delivery Reviews*, 217:115504, 2025. doi: 10.1016/j.addr.2024.115504.

[4] Karabo Innocent Matumba, Teboho Clement Mokhena, Vincent Ojijo, Emmanuel Rotimi Sadiku, and Suprakas Sinha Ray. Morphological characteristics, properties, and applications of polylactide/poly(ε-caprolactone) blends and their composites—a review. *Macromolecular Materials and Engineering*, 309(8):2400056, 2024. doi: 10.1002/mame.202400056.

[5] Ivan Fortelný, Aleksandra Ujčić, Luca Fambri, and Miroslav Slouf. Phase structure, compatibility, and toughness of pla/pcl blends: A review. *Frontiers in Materials*, 6:206, 2019. doi: 10.3389/fmats.2019.00206.

[6] A Ostafinska, I Fortelný, J Hodan, S Krejčíková, M Nevoralová, J Kredatusová, and M Šlouf. Strong synergistic effects in pla/pcl blends: Impact of pla matrix viscosity. *Journal of the Mechanical Behavior of Biomedical Materials*, 69:229–241, 2017.

[7] Solechan Solechan, Agus Suprihanto, Susilo Adi Widyanto, Joko Triyono, Deni Fajar Fitriyana, Januar Parlaungan Siregar, and Tezara Cionita. Investigating the effect of pcl concentrations on the characterization of pla polymeric blends for biomaterial applications. *Materials*, 15(20):7396, 2022.

[8] Kejing Shi, Jonathan P. Salvage, Mohammed Maniruzzaman, and Ali Nokhodchi. Role of release modifiers to modulate drug release from fused deposition modelling (fdm) 3d printed tablets. *International Journal of Pharmaceutics*, 597:120315, 2021. doi: 10.1016/j.ijpharm.2021.120315.

[9] Roberta Censi, Maria Rosa Gigliobianco, Cristina Casadidio, and Piera Di Martino. Hot melt extrusion: Highlighting physicochemical factors to be investigated while designing and optimizing a hot melt extrusion process. *Pharmaceutics*, 10(3):89, 2018.

[10] Sooyeon Chung, Priyanka Srinivasan, Peilun Zhang, Suresh Bandari, and Michael A. Repka. Development of ibuprofen tablet with polyethylene oxide using fused deposition modeling 3d-printing coupled with hot-melt extrusion. *Journal of Drug Delivery Science and Technology*, 76: 103716, 2022. doi: 10.1016/j.jddst.2022.103716.

[11] Preethi Mandati, Dinesh Nyavanandi, Sagar Narala, Abdullah Alzahrani, Sateesh Kumar Vemula, and Michael A. Repka. A comparative assessment of cocrystal and amorphous solid dispersion printlets developed by hot melt extrusion paired fused deposition modeling for dissolution enhancement and stability of ibuprofen. *AAPS PharmSciTech*, 24(7):203, 2023. doi: 10.1208/s12249-023-02666-w.

[12] Hemlata Patil, Roshan V Tiwari, and Michael A Repka. Hot-melt extrusion: from theory to application in pharmaceutical formulation. *AAPS PharmSciTech*, 17(1):20–42, 2016.

[13] Hemlata Patil, Sateesh Kumar Vemula, Sagar Narala, Preethi Lakkala, Siva Ram Munnangi, Nagarjuna Narala, Miguel O. Jara, Robert O. Williams, Hibreniguss Terefe, and Michael A. Repka. Hot-melt extrusion: From theory to application in pharmaceutical formulation—where are we now? *AAPS PharmSciTech*, 25:37, 2024. doi: 10.1208/s12249-024-02749-2.

[14] Omar A Mohamed, Syed H Masood, and Jahar L Bhowmik. Optimization of fused deposition modeling process parameters: a review of current research and future prospects. *Advances in Manufacturing*, 3(1):42–53, 2015.

[15] Mallappa Padmaa Paarakh, Prasanth Anna Jose, Chidambara M Setty, and GV Peterchristoper. Release kinetics–concepts and applications. *International Journal of Pharmacy Research & Technology (IJPRT)*, 8(1):12–20, 2018.

[16] Julen Urquijo, Gonzalo Guerrica-Echevarría, and José Ignacio Eguiazábal. Melt processed pla/pcl blends: Effect of processing method on phase structure, morphology, and mechanical properties. *Journal of Applied Polymer Science*, 132(41), 2015.

[17] Seif Eddine Fenni, Jun Wang, Nacerddine Haddaoui, Basil D. Favis, Alejandro J. Müller, and Dario Cavallo. Crystallization and self-nucleation of pla, pbs and pcl in their immiscible binary and ternary blends. *Thermochimica Acta*, 677:117–130, 2019. doi: 10.1016/j.tca.2019.03.015.

[18] Sanja Mahović Poljaček, Dino Priselac, Tamara Tomašegović, Urška Stanković Elesini, Mirjam Leskovšek, and Mirela Leskovac. Effect of the addition of nano-silica and poly(ε-caprolactone) on the mechanical and thermal properties of poly(lactic acid) blends and possible application in embossing process. *Polymers*, 14(22):4861, 2022. doi: 10.3390/polym14224861.

[19] Marta Przybysz-Romatowska, Mateusz Barczewski, Szymon Mania, Agnieszka Tercjak, Józef Haponiuk, and Krzysztof Formela. Morphology, thermo-mechanical properties and biodegradability of pcl/pla blends reactively compatibilized by different organic peroxides. *Materials*, 14(15):4205, 2021. doi: 10.3390/ma14154205.

[20] Kumaresan Rajan, Mahendran Samykano, Kumaran Kadirgama, Wan Sharuzi Wan Harun, and Md Mustafizur Rahman. Fused deposition modeling: process, materials, parameters, properties, and applications. *The International Journal of Advanced Manufacturing Technology*, 120(3):1531–1570, 2022.

[21] Alberto Boschetto and Luana Bottini. Accuracy prediction in fused deposition modeling. *The International Journal of Advanced Manufacturing Technology*, 73(5):913–928, 2014.

[22] Mahshid Askarizadeh, Narges Esfandiari, Bizhan Honarvar, Seyed Ali Sajadian, and Amin Azdarpour. Kinetic modeling to explain the release of medicine from drug delivery systems. *ChemBioEng Reviews*, 10(6):1006–1049, 2023.